Article

Laboratory Search for Fe IX Solar Diagnostic Lines Using an Electron Beam Ion Trap

Elmar Träbert [1,2,*], Peter Beiersdorfer [2,3], Gregory V. Brown [2], Natalie Hell [2], Jaan K. Lepson [3], Alexander J. Fairchild [4], Michael Hahn [4] and Daniel W. Savin [4]

1 Fakultät für Physik und Astronomie, Ruhr-Universität Bochum, AIRUB, 44780 Bochum, Germany
2 Lawrence Livermore National Laboratory, Physics Division, Livermore, CA 94550-9234, USA
3 Space Sciences Laboratory, University of California, Berkeley, CA 94720, USA
4 Columbia Astrophysics Laboratory, Columbia University, New York, NY 10027, USA
* Correspondence: traebert@astro.rub.de; Tel.: +49-234-3223451; Fax: +49-234-3214169

Abstract: The Fe IX spectrum features two lines in the extreme ultraviolet whose ratio has been rated among the best density diagnostics in the solar spectrum. One line is an $E1$-allowed intercombination transition at 244.909 Å, the other an $E1$-forbidden $M2$ transition at 241.739 Å. Employing a medium and a high resolution spectrometer at the Livermore EBIT-I electron beam ion trap, we have observed the line pair in the laboratory for the first time. Using a CHIANTI model computation, the observed line ratio yields a value of the electron density that is compatible with typical densities in our device.

Keywords: atomic spectra; lifetimes; density diagnostics

1. Introduction

$E1$-forbidden transitions are of great interest in astrophysics, because they can be useful tools in the diagnostics of low-density environments. Among the lowest excited levels in Ar-like ions ($3p^5 3d$), the $^3P^o_{1,2}$ levels connect to the $3p^6$ $^1S_0$ ground level by an $E1$-allowed intercombination transition and an $E1$-forbidden $M2$ transition, respectively. For the highly abundant element Fe, these spectral lines are expected in the extreme ultraviolet (EUV) spectral range. Early calculations by Garstang [1] and Wagner & House [2] provided wavelength estimates of these lines. Garstang moreover calculated the $M2$ transition rate in Fe IX to be close to $70\,\mathrm{s}^{-1}$. Such a low rate implies that the radiative decay can only be observed, if the ion has a chance to decay before it is quenched by collisions. The state-of-the-art of vacuum technology at that time would not permit observation in the laboratory. In the 1960s, sounding rockets and later satellites began to obtain spectra of the solar corona from outside Earth's atmosphere. The first identification of these Fe IX lines in solar corona observations was suggested by Jordan [3]. Svensson, Ekberg and Edlén [4] studied the EUV spectrum of Fe IX in the laboratory (without seeing the $M2$ line) and determined various energy levels with sufficient precision to corroborate Jordan's line identifications. Behring et al. [5] obtained solar spectra by a rocket-borne spectrograph; their wavelength measurements of the two lines of present interest (241.739 Å and 244.909 Å, respectively) remain in the databases [6,7]. Although vacuum techniques have improved significantly since, the $M2$ transition apparently has not yet been reported from the laboratory.

The intensity ratio of the $E1$ intercombination transition to the $M2$ transition can be used as an electron-density plasma diagnostic. Storey & Zeippen [8] rate the two Fe IX lines as having the potential to be among the best density diagnostics in the solar spectrum. The interpretation of density diagnostic line ratios is particularly sensitive to uncertainties in the theoretical atomic data, because they depend on many factors, such as collisional excitation and de-excitation, radiative transition rates, and radiative cascades. Laboratory measurements are needed to benchmark the validity of the theoretical density diagnostic ratios.

The electron beam in the Livermore EBIT-I electron beam ion trap has a typical density of 10^{11} cm^{-3}. This is more than two orders of magnitude lower than the typical electron density in a tokamak plasma device, and it is one to a few orders of magnitude higher than the electron densities found in the quiet solar corona. The radiative transition rate of the $E1$ transition has been calculated to be on the order of 10^7 s^{-1} [9], while for the $M2$ transition rate a value lower than 100 s^{-1} has been predicted [1,9]. In a naive view of line intensities being proportional to the transition rate, a line ratio on the order of 10^5 would be expected in a common laboratory plasma. In actual solar observations, the line ratio has been observed in the range from 1 to 2, which highlights the role of the level population over that of the transition rate in the contributions to the emissivity in such a low-density environment. Different collisional radiative models predict densities that vary by up to an order of magnitude for the same line ratio as a result of different treatments of the population structure. This modelling uncertainty coincides with the rather flat part of the curve for the predicted line ratio in the range of low densities (below $\approx 10^{10}$ cm^{-3}).

Laboratory measurements of this Fe IX line pair would help to resolve this issue. Because of the low radiative $M2$ transition rate, such studies require the very good vacuum of a cryogenic electron beam ion trap to reduce the effects of collisional quenching. The Livermore group has measured atomic level lifetimes in the corresponding 10-ms range with an accuracy of better than 1% [10]. This indicates that the necessary parameters of the measurement environment are being met.

2. Experiment

Our experiment was performed at the EBIT laboratory at Lawrence Livermore National Laboratory, which is the home of EBIT-I and SuperEBIT [11–13]. In these devices, a high density electron beam [14] proceeds in ultrahigh vacuum (UHV) guided by a 3-Tesla magnetic field. The electron beam has an energy spread of less than 50 eV. The electron beam passes along the symmetry axis of a Penning trap, and from the combined magnetic field and drift tube voltages, ions that are produced via electron collision from atoms in the residual gas are trapped. Iron was bled into the trap vessel as iron pentacarbonyl ($Fe(CO_2)_5$), under UHV conditions. The residual gas pressure was about 10^{-11} mbar or better.

Time-integrated soft-X-ray spectra were obtained by using the Long Wavelength Extreme Ultraviolet Spectrometer LoWEUS [15] and the High-resolution Grazing-incidence Grating Spectrometer HiGGS [16]. Both instruments use a cryogenic CCD camera as the (27 mm wide) detector. Figure 1 shows spectra from LoWEUS, obtained at two electron beam energies, one near and one above the expected optimum production of the Fe IX spectrum. The spectrograph has a resolving power $\lambda / \Delta \lambda \approx 500$ in the wavelength range of interest. At the lower electron beam energy, the spectrum in Figure 1 shows lines at the two Fe IX wavelengths, which possibly are partly blended. The high density of spectral lines and the large changes of line intensity with the energy of the exciting electron beam suggest the possible presence of more blending lines than are known from the literature [7,17].

In order to mitigate the issue of line blending, we performed higher resolution measurements with the HiGGS instrument [16]. Sample spectra are shown in Figure 2. The spectra indicate a resolving power of 3000 in the present setting. In order to reach a low electron density that would not quench the long-lived $J = 2$ level, the electron beam current was reduced to a few mA. The CCD was exposed for 60 min, so as to accumulate sufficient signal while not suffering too many cosmic-ray background events. The tracks of the latter were largely removed by filtering the image files. The rather low signal rate is evident in Figure 2 by comparison with the detector background.
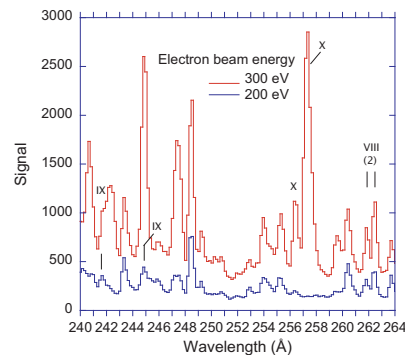
Figure 1. EUV spectra of Fe in the vicinity of the Fe IX lines of interest, obtained with the LoWEUS spectrometer at the Livermore SuperEBIT, using electron beam energies of 200 and 300 eV. Identified spectral lines are marked by the isoelectronic sequence.
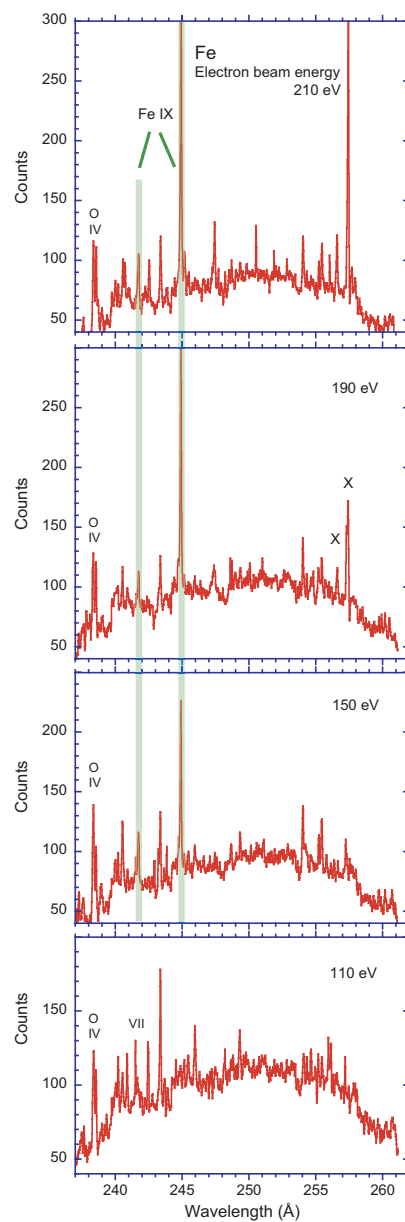

Figure 2. EUV spectra of Fe in the vicinity of the Fe IX lines of interest, obtained with the HiGGS spectrograph at the Livermore EBIT-I electron beam ion trap, using electron beam energies of 110 to 210 eV. Identified Fe lines are marked by the isoelectronic sequence number. The green vertical bars mark the position of the Fe IX lines of present interest.

In one series of measurements, we varied the electron beam energy from 110 eV to 210 eV in order to explore the variations in the spectra, from well below the threshold for producing Fe IX, to near the ionisation potential of Fe VIII (151.06 eV [18]), and to energies beyond. Evidently the Fe IX spectrum is excited with the nominal electron beam energy just below the Fe VIII ionisation threshold. This likely is due to the finite width of the electron beam energy distribution in the beam, resulting in a fraction of the electrons that may exceed the threshold. At the threshold electron beam energy, the spectrum shows relatively more signal around the position of the *M*2 line than is seen at higher electron beam energies. This likely corresponds to the diffuse signal seen in the spectrum recorded at 110 eV (clearly below the threshold for Fe IX production), and is possibly a leftover of the many Fe VII lines known in this wavelength range [7], which must burn out in the presence of more energetic electrons. Additional data were recorded at electron beam energies of 1700 eV and 8050 eV, at which much higher charge states of Fe are reached that have lines suitable for wavelength calibration [17] (Figure 3). Alternatively, carbon dioxide (CO_2) injection served for calibration. The O IV lines at 238.36 Å and 238.57 Å [7,18] appeared with either gas. After a preset time, the trap voltages were altered so that the stored ion cloud was ejected, and a new trapping cycle was started.
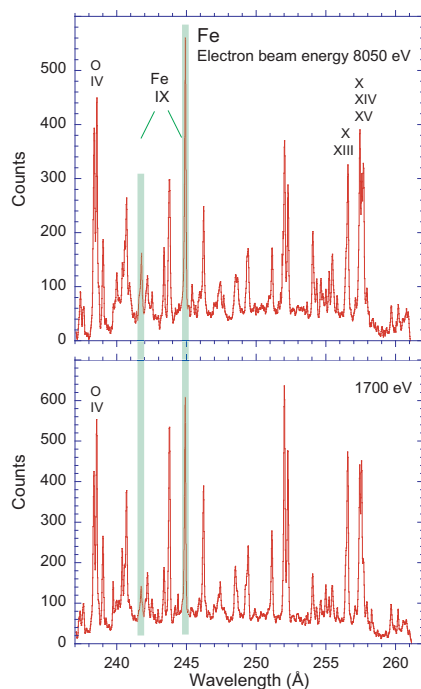

Figure 3. Same as Figure 2, but at higher electron beam energies.

3. Density Dependent Line Ratio

The goal of the experiment was to observe the two Fe IX lines and to determine their line ratio. In a measurement using a grazing-incidence grating spectrograph, the line width is usually dominated by the instrument geometry and the effective slit width, which for these experiments is typically given by the width of the electron beam, and thus it is constant across the spectrum. Consequently, multi-peak fitting for spectrum analysis may be undertaken with a single line profile function (for example, a Gaussian) of a common width. However, we have often observed additional structures at the feet of bright lines that escaped spectral identification, and we have observed lines from the decays of longer-lived excited levels that appeared broader than others. The latter effect is most pronounced among spectral lines in the visible [19]. Arthanayaka et al. [20] have interpreted the broadening by the lateral extent of the trapped ion cloud, which makes for an increased effective entrance slit width of the spectrograph. Excitation is effected by the electron beam in an EBIT, and the emission of light from the decay of short-lived

levels occurs in the same volume (defined by the near 50 μm beam diameter and the ≈2 cm long trap), which can therefore be used as the 'entrance slit' in the slit-less operation of our spectrographs. Actually, the ions in the trap are not confined to the volume of the electron beam; longer-lived levels may decay well after an ion has left the vicinity of the electron beam, while it traverses the trap center on a wider path. The Fe IX *M*2 line, with its long upper-level lifetime (on the order of 14 ms), has no preferred emission zone close to the electron beam trajectory. Consequently, the spatial resolution of our spectrometer was able to resolve the wider emission volume. Because of this single line of higher width, the line intensities were not obtained by multi-peak fitting with a single line width, but by numerical integration over the full line profile above the estimated local background.

The results for the line ratio scatter from about 4 to about 6. The statistical errors of the individual data points are taken from the accumulated signal in each line and from the simple mathematics of calculating a ratio (relative errors add up), including the uncertainty of the background. By averaging, we find an Fe IX line ratio of 4.9 ± 0.2. According to excitation rates given in CHIANTI [21–23], a program and data package widely used, this value corresponds to an electron density n_e of about $2.4 \cdot 10^{10}$ cm^{-3} (see Figure 4), with a statistical uncertainty as small as that of the line ratio. This electron density is compatible with the results of other measurements at this EBIT [24,25]. The above simulation (for more examples, see [25]) uses a Maxwellian electron energy distribution for a temperature of $T = 0.8$ MK, which is the optimum for the production of Fe IX.

The corresponding results from the measurements at 1.7 keV and at 8 keV (Figure 3) are about 20% higher and lower, respectively, and of lower statistical significance so far. Further work is needed on the excitation functions to check for possible line blends that might affect the signal at the higher electron beam energies.
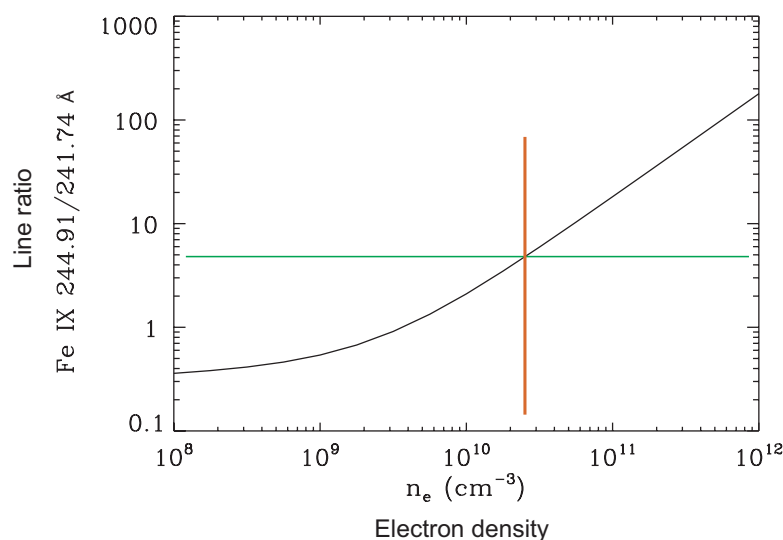

Figure 4. The black curve represents the computed Fe IX line ratio on the basis of CHIANTI v9.0 data [21], as a function of particle density (see [25]). The green horizontal line represents the present line ratio measurement. The orange vertical line indicates the electron density value derived from the theoretical curve.

4. Discussion

The Fe IX line pair of present interest has been claimed to offer a valuable density diagnostic for corona plasmas, yet the different model predictions point to uncertainties in the underlying atomic data used to infer the electron density. Using our laboratory result for the line ratio and the CHIANTI-based model calculation, we present a value for the electron density in our experiment, which is compatible with results that we have obtained by other means [20,24,25]. The CHIANTI model is based on Maxwellian electron energy distributions, whereas the electron beam energy distribution in our experiment does not

have a similar high-energy tail. However, dedicated experiments at this electron beam ion trap have shown that the influence of the (reasonably chosen) specific electron energy distribution on the synthetic spectra is minor. The calculation would be best tested using an independent accurate and precise measure of the effective electron density. We plan to perform such experiments in the near future.

Author Contributions: E.T.: data collection, data evaluation and interpretation, text; P.B.: conceptualisation, funding, data procurement, data evaluation and interpretation, project oversight; G.V.B.: data procurement, text; N.H.: data procurement; J.K.L.: theory, data references and interpretation; A.J.F.: data evaluation and interpretation; M.H.: funding, theory and data treatment; D.W.S.: funding, conceptualisation and oversight. All authors have read and agreed to the published version of the manuscript.

Conflicts of Interest: The authors declare no conflict of interest.

References

1. Garstang, R.H. Magnetic.quadrupole radiation and solar coronal de-excitation. *Proc. Astron. Soc. Pac.* **1969**, *81*, 488–495.
2. Wagner, W.J.; House, L.L. Hartree–Fock calculations of coronal forbidden lines in the Argon I isoelectronic sequence. *Astrophys. J.* **1969**, *155*, 677–686.
3. Jordan, C. Identifications of emission lines in the EUV solar spectrum. *Space Sci. Rev.* **1972**, *13*, 595–605.
4. Svensson, L.Å.; Ekberg, J.O.; Edlén, B. The identification of Fe IX and Ni XI in the solar corona. *Sol. Phys.* **1974**, *34*, 173–179.
5. Behring, W.E.; Cohen, L.; Feldman, U.; Doschek, G.A. The solar spectrum: wavelengths and identifications from 160 to 770 Angstroms. *Astrophys. J.* **1976**, *203*, 521–527.
6. Sugar, J.; Corliss, C. Atomic Energy Levels of the Iron-Period Elements: Potassium through Nickel. *J. Phys. Chem. Ref. Data* **1985**, *14* (Suppl. 2), 1–664.
7. Kramida, A.; Ralchenko, Y.; Reader, J.; NIST ASD Team. *NIST Atomic Spectra Database*, Version 5.9; National Institute of Standards and Technology: Gaithersburg, MD, USA, 2021. Available online: https://physics.nist.gov/asd (accessed on 21 June 2022).
8. Storey, P.J.; Zeippen, C.J. Coronal Fe IX line intensities and electron density diagnostics. *Mon. Not. R. astron. Soc.* **2001**, *324*, L7–L10.
9. Del Zanna, G.; Storey, P.J.; Badnell, N.R.; Mason, H.E. Atomic data for astrophysics: Fe IX. *Astron. Astrophys.* **2014**, *565*, A77.
10. Beiersdorfer, P.; Träbert, E.; Pinnington, E.H. Experimental transition rate of the green coronal line of Fe XIV. *Astrophys. J.* **2003**, *587*, 836–840.
11. Levine, M.A.; Marrs, R.E.; Bardsley, J.N.; Beiersdorfer, P.; Bennett, C.L.; Chen, M.H.; Cowan, T.; Dietrich, D.; Henderson, J.R.; Knapp, D.A.; et al. The use of an electron beam ion trap in the study of highly charged ions. *Nucl. Instrum. Meth. Phys. Res. B* **1989**, *43*, 431–440.
12. Knapp, D.A.; Marrs, R.E.; Elliott, S.R.; Magee, E.W.; Zasadzinski, R. A high-energy electron beam ion trap for production of high-charge high-Z ions. *Nucl. Instrum. Meth. Phys. Res. A* **1993**, *334*, 305–312.
13. Beiersdorfer, P. A "brief" history of spectroscopy on EBIT. *Can. J. Phys.* **2008**, *86*, 1–10.
14. Utter, S.B.; Beiersdorfer, P.; Crespo-López-Urrutia, J.R.; Widmann, K. Position and size of the electron beam in the high-energy electron beam ion trap. *Nucl. Instrum. Meth. Phys. Res. A* **1999**, *428*, 276–283.
15. Lepson, J.K.; Beiersdorfer, P.; Kaita, R.; Majeski, R.; Boyle, D. Responsivity calibration of the LoWEUS spectrometer. *Rev. Sci. Instrum.* **2016**, *87*, 11D614.
16. Beiersdorfer, P.; Magee, E.W.; Brown, G.V.; Hell, N.; Träbert, E.; Widmann, K. Extended-range grazing-incidence spectrometer for high-resolution extreme ultraviolet measurements on an electron beam ion trap. *Rev. Sci. Instrum.* **2014**, *85*, 11E422.
17. Beiersdorfer, P.; Lepson, J.K. Measurement of the Fe VIII–Fe XVI 3–3 emission in the extreme ultraviolet and comparison with CHIANTI. *Astrophys. J. Suppl. Ser.* **2012**, *201*, 28.
18. Kelly, R.L. Atomic and ionic spectrum lines below 2000 Angstroms: Hydrogen through krypton. *J. Phys. Chem. Ref. Data* **1987**, *16* (Suppl. 1), 1–659.
19. Crespo López-Urrutia, J.R.; Beiersdorfer, P.; Widmann, K.; Decaux, V. Visible spectrum of highly charged ions: The forbidden optical lines of Kr, Xe, and Ba ions in the Ar I to Kr I isoelectronic sequence. *Can. J. Phys.* **2002**, *80*, 1687–1700.
20. Arthanayaka, T.; Beiersdorfer, P.; Brown, G.V.; Hahn, M.; Hell, N.; Lockard, T.E.; Savin, D.W. Measurements of the effective electron density in an electron beam ion trap using extreme ultraviolet spectra and optical imaging. *Rev. Sci. Instrum.* **2018**, *89*, 10E119.
21. Dere, K.P.; DelZanna, G.; Young, P.R.; Landi, E.; Sutherland, R. CHIANTI - An atomic database for emission lines: Improvements for the X-ray satellite lines. *Astrophys. J. Suppl. Ser.* **2019**, *241*, 2.

22.   Del Zanna, G.; Dere, K.P.; Young, P.R.; Landi, E.; Mason, H.E. CHIANTI—An atomic database for emission lines. Version 8. *Astron. Astrophys.* **2015**, *582*, 56.

23.   Del Zanna, G.; Young, P.R. Atomic data for plasma spectroscopy: The CHIANTI database, improvements and challenges. *Atoms* **2020**, *8*, 46.

24.   Chen, H.; Beiersdorfer, P.; Gu, M.-F.; Heeter, L.A.; Lepson, J.K.; Liedahl, D.A.; Naranjo-Rivera, K.L.; Träbert, E. Experimental and theoretical evaluation of density-sensitive N VI, Ar XIV, and Fe XXII line ratios. *Astrophys. J.* **2004**, *611*, 598–604.

25.   Arthanayaka, T.; Beiersdorfer, P.; Brown, G.V.; Gu, M.F.; Hahn, M.; Hell, N.; Lockard, T.E.; Savin, D.W. Laboratory calibrations of Fe XII–XIV line-intensity ratios for electron density diagnostics. *Astrophys. J.* **2020**, *890*, 77.